J Solid State Electrochem (2011) 15:1901–1907
DOI 10.1007/s10008-010-1206-6

ORIGINAL PAPER

Preparation and electrochemical performance of nano-structured $Li_2Mn_4O_9$ for supercapacitor

Yan-Jing Hao · Ling Wang · Qiong-Yu Lai

Received: 18 June 2010 / Revised: 19 September 2010 / Accepted: 20 September 2010 / Published online: 13 October 2010

Abstract Nano-structured spinel $Li_2Mn_4O_9$ powder was prepared via a combustion method with hydrated lithium acetate ($LiAc{\cdot}2H_2O$), manganese acetate ($MnAc_2{\cdot}4H_2O$), and oxalic acid ($C_2H_2O_4{\cdot}2H_2O$) as raw materials, followed by calcination of the precursor at 300 °C. The sample was characterized by X-ray diffraction, scanning electron microscope, and energy-dispersive X-ray spectroscopy techniques. Electrochemical performance of the nano-$Li_2Mn_4O_9$ material was studied using cyclic voltammetry, ac impedance, and galvanostatic charge/discharge methods in 2 $mol L^{-1}$ $LiNO_3$ aqueous electrolyte. The results indicated that the nano-$Li_2Mn_4O_9$ material exhibited excellent electrochemical performance in terms of specific capacity, cycle life, and charge/discharge stability, as evidenced by the charge/discharge results. For example, specific capacitance of the single $Li_2Mn_4O_9$ electrode reached 407 $F g^{-1}$ at the scan rates of 5 $mV s^{-1}$. The capacitor, which is composed of activated carbon negative electrode and $Li_2Mn_4O_9$ positive electrode, also exhibits an excellent cycling performance in potential range of 0–1.6 V and keeps over 98% of the maximum capacitance even after 4,000 cycles.

Keywords Supercapacitor · Nano-structured $Li_2Mn_4O_9$ · Electrochemical performance · Aqueous electrolyte · Long cycle life

Y.-J. Hao (✉) · L. Wang · Q.-Y. Lai
College of Chemistry, Sichuan University,
Chengdu 610064, People's Republic of China
e-mail: haoyanjing@yahoo.com

Introduction

Supercapacitor is a promising candidate for power sources of electric vehicles due to its high power density. Traditional double-layer supercapacitor is based on activated carbon (AC) or other similar materials. However, the energy density of double-layer AC/AC system is low (3–6 $Wh kg^{-1}$). Today, much research in electrochemical capacitors aims to increase power and energy density as well as reduce fabrication cost while using environmental friendly materials [1–3]. One of the most useful approaches is to develop a hybrid system that typically consists of an electrochemical double-layer capacitor electrode and a battery electrode, such as AC/$Ni(OH)_2$, AC/MnO_2, AC/$LiTi_2(PO_4)_3$, AC/$Li_4Mn_5O_{12,}$ and AC/$LiMn_2O_4$ systems [4–8]. Both the increase of the working voltage and the high energy density of the battery electrode material result in a significant increase in the overall energy density of the capacitors compared with that of AC/AC system.

Recently, we have demonstrated that the high cation-deficiency $Li_2Mn_4O_9$ material exhibited excellent electrochemical performance in aqueous electrolytes [9]. We were interested in it because spinel $Li_2Mn_4O_9$ is a very peculiar case in the Li–Mn–O system. This compound contains cation vacancies on both tetrahedral and octahedral sites [10–12]. Such a high cation deficiency could lead to high lithium intercalation capacity [11, 13–16]. It is well known that the performance of the powders used as electrode materials in supercapacitor or lithium-ion batteries is strongly affected by their preparation processes, so it is very important to select a suitable method to prepare high-performance $Li_2Mn_4O_9$. Nano-structured materials, because of their unique characters, show remarkable properties in the energy storage applications. They have the advantages of large specific area, wider charge/discharge potential

range, and higher specific capacitance, which attract much attention in the world as electrode material for supercapacitors in recent years [17–19].

The precursor materials reported in the literature for the solid state synthesis of $Li_2Mn_4O_9$ [11, 16] are usually oxides, hydroxides, carbonates, or nitrates of manganese and lithium. We report here on the synthesis of nanostructured $Li_2Mn_4O_9$ using an oxalic acid-assisted combustion method. The stoichiometry elemental analysis of Mn and O was determined by energy-dispersive X-ray spectroscopy (EDS). The electrochemical behavior of the material was demonstrated using simulative aqueous supercapacitor, in which AC was used as anode material, nanostructured $Li_2Mn_4O_9$ as cathode material, and 2 $molL^{-1}$ $LiNO_3$ aqueous solution as electrolyte.

Experimental

All chemicals were obtained from commercial sources and used without further purification. The $Li_2Mn_4O_9$ was synthesized by the following procedure. Stoichiometric amount of $Li(CH_3COO)_2{\cdot}2H_2O$ (AR), $Mn(CH_3COO)_2{\cdot}4H_2O$ (AR), and a certain amount of oxalic acid (the molar ratio of oxalic acid to total metal ions was 1:1) were mixed together. The mixture was ground sufficiently in a ceramic mortar for about 1 h until the mixture changed to a light pink viscous complex intermediate. The mixture was dried at 75 °C under vacuum to obtain manganese oxide precursor. The precursor was then preheated at 300 °C in air for 2 h to decompose the organic components and further calcined at 300 °C for 8 h to obtain the final product. The AC was used as received (provided by Shanghai Aowei Technology Development Company Limited, China) and had a BET surface area of about 1,500 m^2g^{-1}.

Powder X-ray diffraction (XRD) data were collected on a Rigaku D/MAX-rA diffractometer with CuK α radiation (λ=1.5418 nm), operating at 40 kV and 100 mA. The scanning electron microscope (SEM, JSM-5900LV, Japan) was used to observe the morphology and particle size. The chemical composition of the compound was confirmed by a field emission scanning electron microscope (JSM6700F) equipped with an EDS (Oxford INCA).

The $Li_2Mn_4O_9$ electrode was prepared by mixing 75 wt % active material, 20 wt% acetylene black and 5 wt% polyvinylidene fluoride (PVDF) binder together using N-methyl-2-pyrrolidine as the solvent. After drying the obtained mixture slurry overnight under vacuum at 80 °C, the mixture was pressed onto a stainless steel grid to obtain the $Li_2Mn_4O_9$ electrode. The preparation of AC electrode was similar to that of $Li_2Mn_4O_9$ electrode. The ratio of AC, acetylene black, and PVDF was 65:30:5 (wt.%).

Cyclic voltammetry (CV) were carried out in a three-electrode glass cell in 2 $molL^{-1}$ $LiNO_3$ electrolyte using a LK2005 electrochemical workstation system. Platinum foil was used as a counter electrode, and saturated calomel electrode (SCE, 0.242 V) as the reference electrode. Charge/discharge test of hybrid capacitor was performed using a two-electrode glass cell consisting of $Li_2Mn_4O_9$ positive electrode and activated carbon negative electrode with Neware Battery Program-control Testing System. Electrochemical impedance measurements were performed on an Autolab PGSTAT 12 potentiostat (Amsterdam, The Netherlands) using a three-electrode system in which platinum foil and SCE were used as the counter and reference electrodes.

Results and discussion

$Li_2Mn_4O_9$ is a high cation-deficiency spinel material [10]. The crystal structure of spinel $Li_2Mn_4O_9$ is depicted in Fig. 1. The MnO_6 octahedra share edges with six octahedral-site neighbors, two of which are located in the same plane and the remaining four are above and below the plane. The LiO_4 tetrahedral sites share corners with octahedral sites. In the $Li_2Mn_4O_9$ spinel matrix, lithium ions are located at the tetrahedral 8a sites, manganese ions are distributed at the octahedral 16d sites, and the oxygen ions occupy the 32e sites. Both the tetrahedral and octahedral sites contain cation vacancies. Cock [10] deduced that the spinel $Li_2Mn_4O_9$ possesses the structural formula of $\left(Li_{8/91/9}\right)\left[Mn_{16/92/9}\right]O_4$, in which □ (white square) indicates vacancy in the tetrahedral and octahedral sites.

Figure 2 shows the X-ray diffraction patterns of $Li_2Mn_4O_9$ powders. The calculated unit parameter of a= 8.1592 Å is very close to the previous results obtained by Kostecki et al. [20]. The crystallite size of $Li_2Mn_4O_9$ calculated by the Scherrer's formula from (1 1 1) diffraction

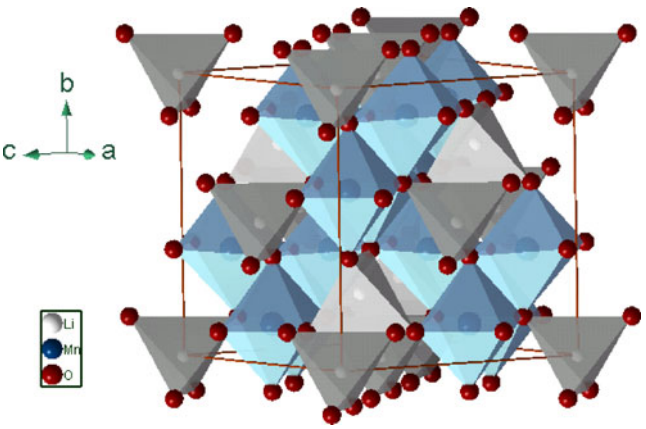

Fig. 1 Crystal structure of spinel $Li_2Mn_4O_9$

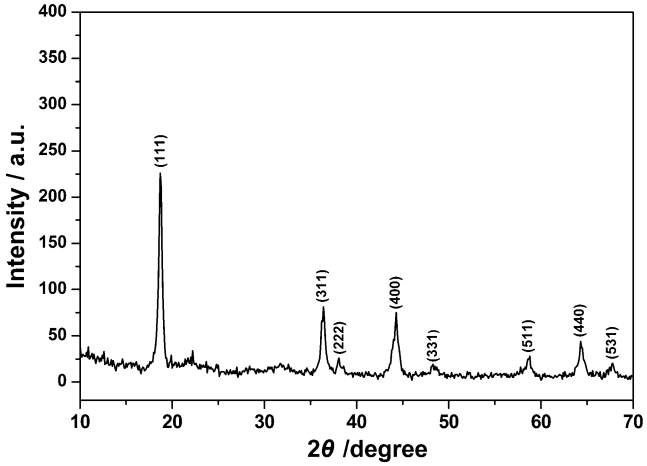

Fig. 2 X-ray diffraction pattern of nano-$Li_2Mn_4O_9$ sample

peak is about 29 nm. In addition, all the diffraction peaks can be indexed in the space group *Fd3m* (JCPDS No. 88–1608) of a cubic spinel, indicating that $Li_2Mn_4O_9$ pure phase formed [21].

However, it is difficult to prepare fully oxidized spinel $Li_2Mn_4O_9$ as is well known [12]. Strict control of experimental conditions such as temperature, time, and particle size of the precursor materials is essential for producing fully oxidized, single-phase material. By studies to date, the fully oxidized $Li_2Mn_4O_9$ phase has never been prepared successfully. The value of z in $Li_2Mn_4O_{8+z}$ has generally been reported to be in the range of 0.2 to 0.5 [22, 23]. In order to determine the elemental ratio of Mn and O, EDS analysis was performed (Fig. 3). Results of EDS microprobe elemental analyses on $Li_2Mn_4O_9$ gave a molar ratio of about 4:8.39 for Mn:O. That means the value of z in $Li_2Mn_4O_{8+z}$ is about 0.39, which is close to the highest value reported in the literature [22, 23].

Figure 4a and b show SEM images of $Li_2Mn_4O_9$ sample prepared by combustion process with low and high magnifications, respectively. The images clearly show that $Li_2Mn_4O_9$ sample is composed of many small nano grains with the average particle size of about 50 nm without agglomeration. In our previous work [24], we synthesized $Li_4Ti_5O_{12}$ with oxalic acid as a chelating agent and a fuel and found that oxalic acid played an important role in the formation of nano Li–Ti–O material. According to our previously study, oxalic acid forms a mixed precursor, which acts as a substrate for the homogeneous distribution of the metal oxide phase. Upon calcination in air, the carbonaceous substrate is oxidized to carbon dioxide, leaving behind a finely divided oxide phase. In this case, oxalic acid had the similar effect.

Figure 5 show the cyclic voltammograms curves of $Li_2Mn_4O_9$ electrodes in various potential ranges at a scan rate of 5 mVs^{-1} in 2 $molL^{-1}$ $LiNO_3$ aqueous solution. It is clearly shown that no peaks of the H_2 and O_2 evolution are found in the widest potential range of 0 to 1.4 V, indicating that capacitive performance of the $Li_2Mn_4O_9$ electrode is stable in the potential limits. When potential voltage is in

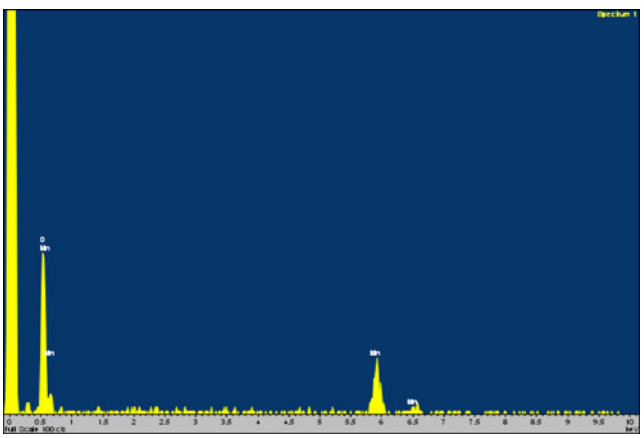

Fig. 3 Energy-dispersive X-ray spectroscopy of nano-$Li_2Mn_4O_9$ sample

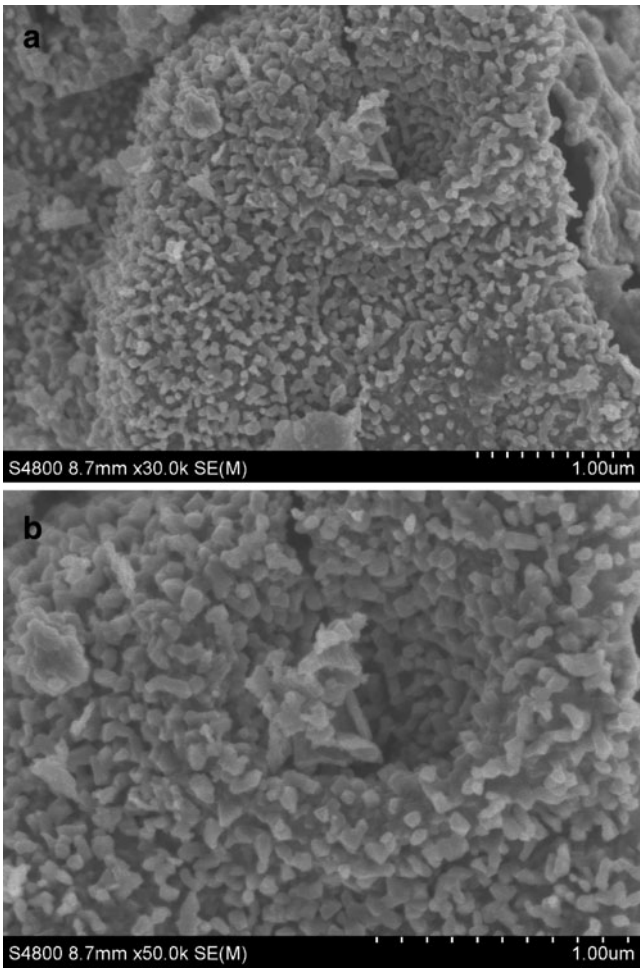

Fig. 4 SEM graph of nano-structured $Li_2Mn_4O_9$ with **a** low and **b** high magnifications

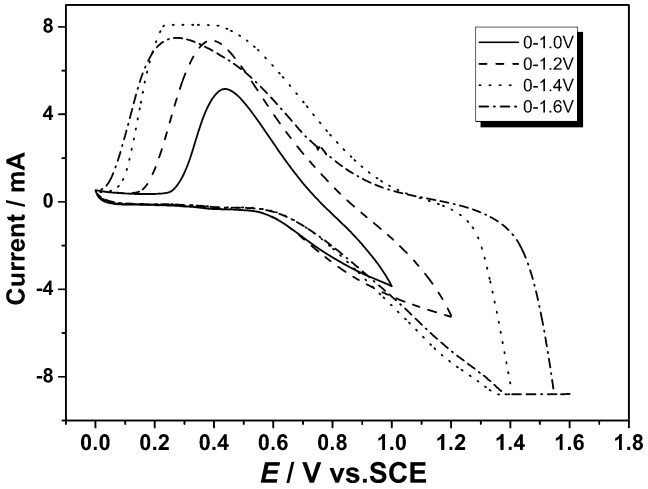

Fig. 5 CV curves of nano-$Li_2Mn_4O_9$ electrode in different potential ranges at a scan rate of 5 mVs^{-1}

0–1.4 V (vs. SCE), the electrode exhibits the best capacitive performance. The oxidation/reduction peak-potential centered at 0.5 and 1.2 V (potential vs. SCE) suggests that the reaction of $Li_2Mn_4O_9$ electrode in aqueous Li salt electrolyte is a quasi-reversible Li^+ insertion/extraction process, which is in good agreement with the extraction/insertion reaction of $Li_2Mn_4O_9$ in the organic electrolyte [12]. Faradic redox reaction occurred both on the surface and in the inner matrix of the $Li_2Mn_4O_9$ material and this could provide high pseudocapacitance [9].

According to the cyclic voltammetry, the specific capacitance of the single $Li_2Mn_4O_9$ electrode was calculated by the following equation [8]:

$$C = \frac{Q}{2m \cdot \Delta V}, \quad (1)$$

where Q refers to the charge integrated from the cathodic sweep, ΔV and m refer to the difference in the voltage window and weight of the single $Li_2Mn_4O_9$ electrode, respectively. According to the equation, specific capacitances of the single $Li_2Mn_4O_9$ electrode were calculated to be 407 Fg^{-1} during 0–1.4 V at the scan rates of 5 mVs^{-1}. This is a relatively high value for supercapacitor electrode materials. It is lower than that of mesoporous MnO_2 (a maximum capacitance of 449 Fg^{-1}) [25] and PSC–Co_3O_4 electrode (a maximum capacitance of 453 Fg^{-1}) [26], but higher than most of other electrode materials. For example, a maximum specific capacitance of 344 Fg^{-1} was obtained for the layered structure MnO_2 [27]. A hydrothermally prepared nano-structured MnO_2 showed a high specific capacitance of 168 Fg^{-1} [28]. Hydrous ruthenium dioxide ($RuO_2 \cdot xH_2O$) prepared in a modified sol–gel process by Chang et al. [29] delivered a specific capacitance of 390 Fg^{-1}. A chemically deposited nanocrystalline NiO thin films showed maximum specific capacitance of 167 Fg^{-1} [30].

According to the result obtained from the SEM, the sample synthesized by an oxalic acid combustion method had nano-structured particles. It is well known that the particle size, shape, and homogeneity of electrode materials have a definite effect on the electrochemical properties. Among them, particle size is the main factor. According to Singhal et al. [31], smaller particles have shorter diffusion distances for intercalated Li-ions, resulting in a higher charge rate for intercalated electrode materials. Since electrochemical lithium intercalation and deintercalation are in general limited by the rate of diffusion. The aforementioned features are important because smaller grain size can favor the lithium-ion mobility in the particles

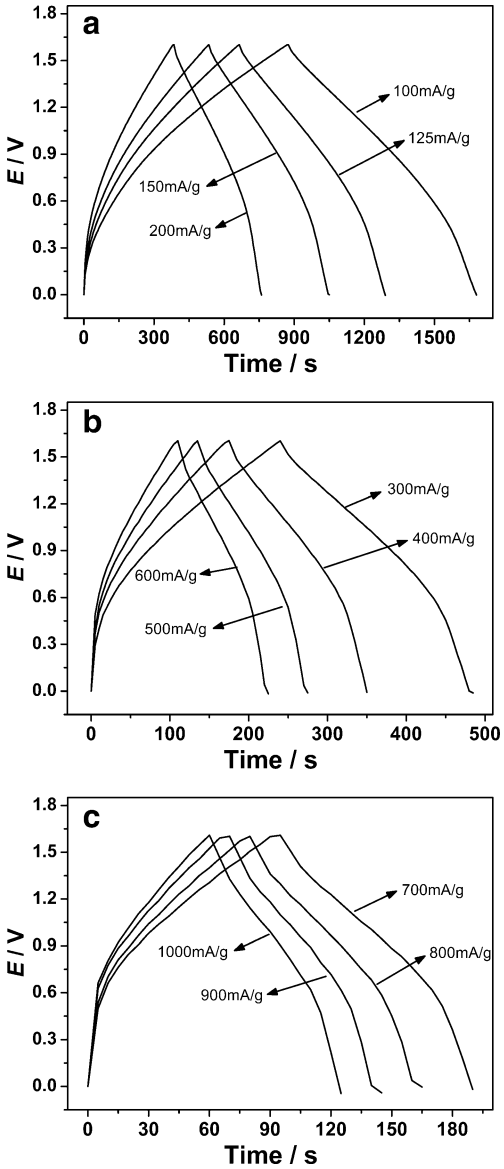

Fig. 6 a–c Galvanostatic charge/discharge curves of the AC/$Li_2Mn_4O_9$ hybrid aqueous capacitor in 2 $molL^{-1}$ $LiNO_3$ between 0 and 1.6 V at various current rates

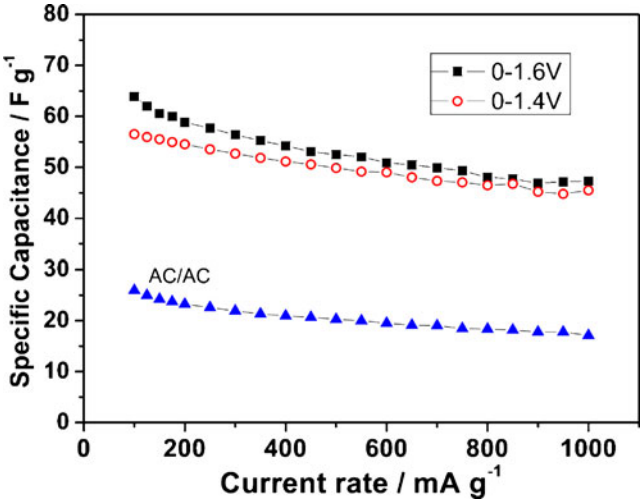

Fig. 7 Specific capacitance of the AC/$Li_2Mn_4O_9$ hybrid capacitor and AC/AC symmetric capacitor at different current rate

by reducing the ion-diffusion pathway and the active material could be utilized sufficiently.

Figure 6a–c shows the galvanostatic charge/discharge curves of the AC/$Li_2Mn_4O_9$ hybrid aqueous supercapacitor in 2 molL^{-1} $LiNO_3$ between 0 and 1.6 V at various current rates from 100 to 1,000 mAg^{-1}. The curves are almost linear and there is no obvious sudden drop of potential at the beginning of charge and discharge observed due to the ohmic resistance of the cell. Figure 7 gives the changes of specific capacitance of the AC/$Li_2Mn_4O_9$ hybrid supercapacitor dependence on charge/discharge current rates. The discharge specific capacitance of the supercapacitor was calculated according to the following equation:

$$C = \frac{I \times \Delta t}{\Delta V \times m}, \tag{2}$$

where I is the discharge current, ΔV is the discharge voltage, Δt is the discharge time, m is the total mass of active materials including positive and negative electrodes in the supercapacitor.

In potential range of 0–1.6 V, the specific capacitance of AC/$Li_2Mn_4O_9$ asymmetric capacitor decreases from 64 Fg^{-1} at a current rate of 100 mAg^{-1} to 47 Fg^{-1} at 1,000 mAg^{-1}. In potential range of 0–1.4 V, the capacitance decreases from 57 Fg^{-1} at 100 mAg^{-1} to 45 Fg^{-1} at 1,000 mAg^{-1}. When current rate increases, specific capacitance of the hybrid supercapacitor decreases slowly. The results suggest that the AC/$Li_2Mn_4O_9$ hybrid capacitor presents excellent rate capability in the above working windows. The AC/$Li_2Mn_4O_9$ hybrid capacitor also has a good specific energy density and power density. For example, in potential range of 0–1.6 V, the specific energy is 22.8 Whkg^{-1} at a power density of about 100 Wkg^{-1} and still keeps 16.7 Whkg^{-1} at a power density of 1,000 Wkg^{-1}. For comparison, the specific capacitance change of AC/AC symmetric supercapacitor in potential range of 0–1.6 V is also listed. As seen in the figure, the capacitance decreases from 26 Fg^{-1} at 100 mAg^{-1} to 17 Fg^{-1} at 1,000 mAg^{-1}, which is much lower than the value of AC/$Li_2Mn_4O_9$ hybrid capacitor.

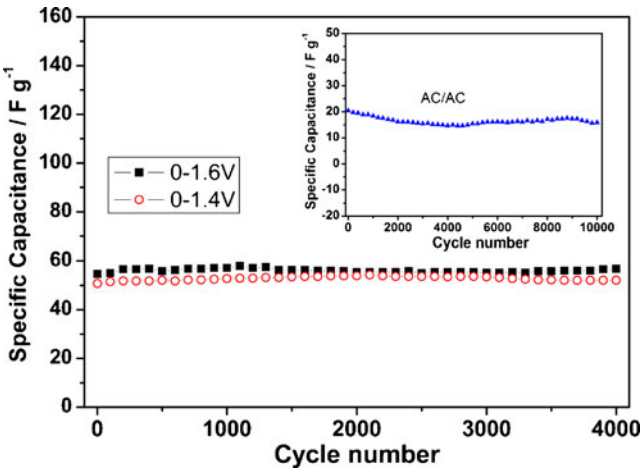

Fig. 8 Cycling behavior of the AC/$Li_2Mn_4O_9$ capacitor and AC/AC symmetric capacitor in 2 molL^{-1} $LiNO_3$ at a current rate of 300 mAg^{-1}

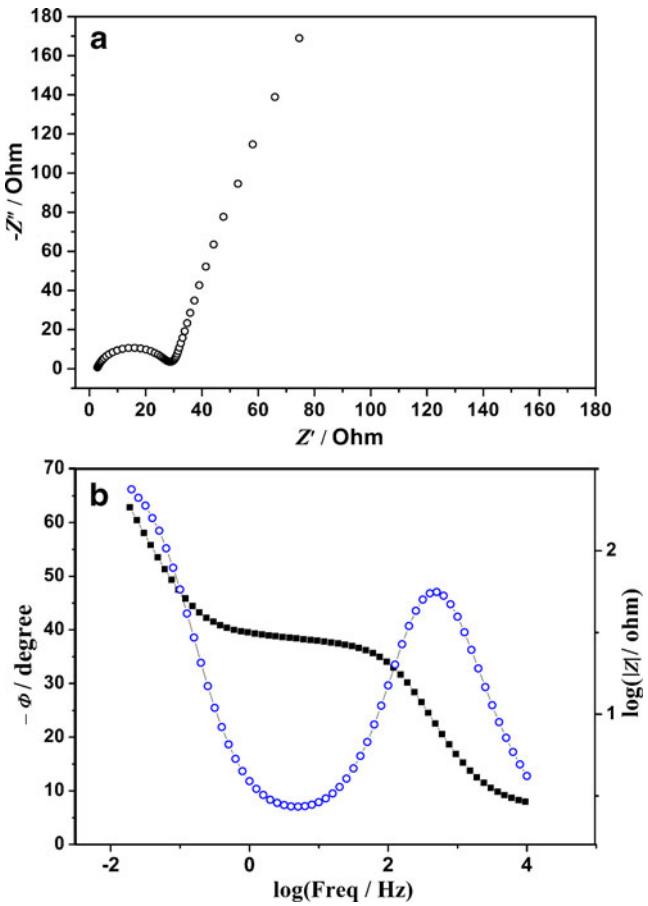

Fig. 9 **a** Impedance spectra. **b** Bode plots of $Li_2Mn_4O_9$ electrode in 2 molL^{-1} $LiNO_3$ solution

The cycling stability of the AC/$Li_2Mn_4O_9$ hybrid supercapacitor upon charge/discharge cycling was tested in 2 molL^{-1} $LiNO_3$ at a current rate of 300 mAg^{-1} as is illustrated in Fig. 8. The hybrid supercapacitor exhibited an excellent cycle profile and maintained over 98% of its maximum specific capacitance after 4,000 cycles between 0 and 1.6 V. The capacitor also exhibits an excellent cycling performance and keeps over 96% of the maximum capacitance after 4,000 cycles in potential range of 0–1.4 V. Cycling behavior of AC/AC symmetric supercapacitor in 2 molL^{-1} $LiNO_3$ is also shown in inset of Fig. 8. The maximum specific capacitance at 300 mAg^{-1} is 20.4 Fg^{-1} and it keeps 15.9 Fg^{-1} after 10,000 cycles. The AC/AC symmetric supercapacitor also has excellent cycling performance in $LiNO_3$ electrolyte, but the specific capacitance is much lower than that of AC/$Li_2Mn_4O_9$ hybrid capacitor. The results show that nano-$Li_2Mn_4O_9$ electrode plays a key role in the hybrid supercapacitor. It provides a high specific capacitance for the capacitor and maintains excellent cycling performance at the same time.

Figure 9a shows the impedance plot of the $Li_2Mn_4O_9$ electrode in 2 molL^{-1} $LiNO_3$ solution. The plot is composed of a semicircle and a straight line. The semicircle at high frequency region should be attributed to the charge transfer process at electrode/electrolyte interface, and the straight line at lower frequency region should be ascribed to the diffusion process in solid [32]. The semicircle is small, indicating that the electrochemical reaction resistance for $Li_2Mn_4O_9$ electrode in 2 molL^{-1} $LiNO_3$ electrolyte is small. The Bode plots for the $Li_2Mn_4O_9$ electrode is shown in Fig. 9b. As can be seen in the figure, the total impedance increased with decreasing in the frequency. In the lower frequency (0.01 Hz), the negative values of the phase angle reach −65° for the $Li_2Mn_4O_9$ electrode. Both of the results indicate that the nano-$Li_2Mn_4O_9$ electrode has good capacitive performance.

Conclusions

A nano-structured $Li_2Mn_4O_9$ material for supercapacitor has been synthesized by an oxalic acid-assisted combustion method, and characterized by XRD, EDS analysis, and SEM observation. CV results indicate that the nano-structured $Li_2Mn_4O_9$ material exhibits a high specific capacitance of 407 Fg^{-1} at a scan rate of 5 mVs^{-1}. Charge/discharge tests show that hybrid AC/$Li_2Mn_4O_9$ supercapacitor possessed excellent rate capability and long cycle life in 2 molL^{-1} $LiNO_3$ aqueous electrolyte. The hybrid capacitor delivered a maximum discharge capacitance of 64 Fg^{-1} at the current density of 100 mAg^{-1} and remained 47 Fg^{-1} at 1,000 mAg^{-1}, which is much higher than the value of AC/AC symmetric supercapacitor. After 4,000 cycles, it still remained above 98% of its initial capacitance. EIS impedance result demonstrated that the charge transfer resistance for the nano-$Li_2Mn_4O_9$ electrode is small. The nano-$Li_2Mn_4O_9$ material is a promising candidate for the power sources of electric vehicles and other large power devices owning to its low price, non-toxicity, long cycle life, excellent rate behavior, and easy preparation.

Acknowledgement The authors acknowledge the financial support from the National Natural Science Foundation of China (no. 20701029).

References

1. Conway BE, Birss V, Wojtowicz J (1997) J Power Sources 66:1–14
2. Conway BE (1991) J Electrochem Soc 138:1539–1548
3. Sarangapani S, Tilak BV, Chen CP (1996) J Electrochem Soc 143:3791–3799
4. Lika SM, Reisner DE, Dai J, Cepulis R (2001) Proceedings of the 11th International Seminar on Double Layer Capacitors, Florida Educational Seminars Inc.
5. Brousse T, Toupin M, Belanger D (2004) J Electrochem Soc 151: A614–A622
6. Wang YG, Luo JY, Wang CX, Xia YY (2006) J Electrochem Soc 153:A1425–A1431
7. Luo JY, Liu JL, He P, Xia YY (2008) Electrochim Acta 53:8128–8133
8. Hao YJ, Wang YY, Lai QY, Zhao Y, Chen LM, Ji XY (2009) J Solid State Electrochem 13:905–912
9. Hao YJ, Lai QY, Wang L, Xu XY, Chu HY (2010) Synth Met 160:669–674
10. de Kock A, Rossouw MH, de Picciotto LA, Thackeray MM (1990) Mater Res Bull 25:657–664
11. Strobel P, Ibarra Palos A, Anne M (2001) J Power Sources 97–98:381–384
12. Masquelier C, Tabuchi M, Ado K, Kanno R, Kobayashi Y, Maki Y, Nakamura O, Goodenough JB (1996) J Solid State Chem 123:255–266
13. Kilroy WP, Ferrando WA, Dallek S (2001) J Power Sources 97–98:336–343
14. Xia YY, Yoshio M (1996) J Power Sources 63:97–102
15. Wang GX, Zhong S, Bradhurst DH, Dou SX, Liu HK (1998) J Power Sources 74:198–201
16. Ibarra Palos A, Anne M, Strobel P (2001) J Solid State Chem 160:108–117
17. Arumugam D, Paruthimal Kalaignan G, Manisankar P (2009) J Solid State Electrochem 13:301–307
18. Wang J, Wang G, Yang L, Ng SH, Liu H (2006) J Solid State Electrochem 10:250–254
19. Farsi H, Gobal F (2007) J Solid State Electrochem 11:1085–1092
20. Kostecki R, Kong F, Matsuo Y, McLarnon F (1999) Electrochim Acta 45:225–233
21. Masquelier C, Tabuchi M, Ado K (1996) J Solid State Chem 123:255–266
22. Xia Y, Yoshio M (1997) J Electrochem Soc 144:4186–4194
23. Dallek S (1998) Characterization of Li2Mn4O9 Cathode Material by Thermogravimetry. In: Proceeding of the 38th Power Sources Conference, 8–11 June 1998, pp 378–381
24. Hao YJ, Lai QY, Lu JZ, Wang HL, Chen YD, Ji XY (2006) J Power Sources 158:1358–1364

25. Xue T, Xu CL, Zhao DD, Li XH, Li HL (2007) J Power Sources 164:953
26. Li Y, Huang K, Liu S, Yao Z, Zhuang S. J Solid State Electrochem. doi:10.1007/s10008-010-1128-3
27. Zolfaghari A, Ataherian F, Ghaemi M, Gholami A (2007) Electrochim Acta 52:2806–2814
28. Subramanian V, Zhu H, Wei B (2006) J Power Sources 159:361–364
29. Chang K-H, Hu C-C, Chou C-Y (2009) Electrochim Acta 54:978–983
30. Patil UM, Salunkhe RR, Gurav KV, Lokhande CD (2008) Appl Surf Sci 255:2603–2607
31. Singhal A, Skandan G, Amatucci G (2004) J Power Sources 129:38–44
32. Liu L, Wang W, Zou W, He B, Sun M, Wang M, Xu X (2007) J Solid State Electrochem. doi:10.1007/s10008-010-1051-7